

# Optimizing protein V untranslated region sequence in M13 phage for increased production of single-stranded DNA for origami

Bo-Young Lee<sup>1,†</sup>, Jaewon Lee<sup>2,†</sup>, Dong June Ahn<sup>1,2,3,4</sup>, Seungwoo Lee<sup>2,3,4,\*</sup> and Min-Kyu Oh<sup>1,4,\*</sup>

<sup>1</sup>Department of Chemical & Biological Engineering, Korea University, Seoul 02841, Republic of Korea, <sup>2</sup>KU-KIST Graduate School of Converging Science and Technology, Korea University, Seoul 02841, Republic of Korea, <sup>3</sup>Department of Integrative Energy Engineering, Korea University, Seoul 02841, Republic of Korea and <sup>4</sup>The w: Interface Augmentation Center, Korea University, Seoul, 02841, Republic of Korea

Received January 06, 2021; Revised April 30, 2021; Editorial Decision May 11, 2021; Accepted May 21, 2021

## ABSTRACT

DNA origami requires long scaffold DNA to be aligned with the guidance of short staple DNA strands. Scaffold DNA is produced in *Escherichia coli* as a form of the M13 bacteriophage by rolling circle amplification (RCA). This study shows that RCA can be reconfigured by reducing phage protein V (pV) expression, improving the production throughput of scaffold DNA by at least 5.66-fold. The change in pV expression was executed by modifying the untranslated region sequence and monitored using a reporter green fluorescence protein fused to pV. In a separate experiment, pV expression was controlled by an inducer. In both experiments, reduced pV expression was correlated with improved M13 bacteriophage production. High-cell-density cultivation was attempted for mass scaffold DNA production, and the produced scaffold DNA was successfully folded into a barrel shape without compromising structural quality. This result suggested that scaffold DNA production throughput can be significantly improved by reprogramming the RCA in *E. coli*.

## INTRODUCTION

DNA origami, in which a long single-stranded DNA (ssDNA) scaffold is folded into a custom-nanoscale shape with the guidance of multiple short DNA staple strands, introduces a versatile but deterministic molecular pegboard with a resolution of a few nanometers (~5 nm) (1–7). In particular, the exotic modularity of staple strands can integrate regularly arrayed and highly dense ssDNA handles into two- or three-dimensionally parallelized double helices (i.e. DNA

origami), which in turn promotes their transformative applications, including as nanomachines (8–10), drug delivery systems (11–13), and in nanophotonics (14–16). Nevertheless, performing DNA origami and its relevant translation into practical applications has not yet become popular, mainly because of the limited access to and high cost of obtaining sufficient amounts of scaffold. The high synthesis cost for staple DNA production, which is another major obstacle, has been effectively addressed through biotechnological production of phagemids with self-excising DNAzyme cassettes (i.e., encoding all staple and scaffold DNA on one phagemid) (17). However, this well-established biotechnological mass production protocol has been limited to relatively small DNA origami based on 3200 bases (€0.18/mg); relatively long single-stranded DNA (7000–8600 bases) can still be viewed as a commodity scaffold in overall DNA origami society. For example, most DNA origami studies, reported thus far, have depended on only one scaffold DNA (i.e. 7249 bases; p7249), mainly because it is commercially available. Nevertheless, such biotechnological production strategy is not yet elucidated for this commodity scaffold. The scaffold DNA from the M13 phage can be produced in *Escherichia coli* harboring F pili. To customize the production of scaffold DNA with efficient throughput, high cell density fermentation (*E. coli*) with optimization of variables (e.g. temperature, media composition, and freeing regiments) has previously been proposed (18–24). However, to facilitate the rapid uptake of DNA origami for newcomers and experts alike, scaffold DNA production, which enables improved throughput, needs to be further diversified without compromising DNA folding quality.

The M13 phage is a virus infecting *E. coli* and has its own replication system independent to the host's system, called rolling circle amplification (RCA) (18). When the

\*To whom correspondence should be addressed. Tel: +82 2 3290 3308; Fax: +82 2 926 6102; Email: mkoh@korea.ac.kr  
Correspondence may also be addressed to Seungwoo Lee. Tel: +82 2 3290 4617; Fax: +82 2 921 0688; Email: seungwoo@korea.ac.kr

<sup>†</sup>The authors wish it to be known that, in their opinion, the first two authors should be regarded as Joint First Authors.

M13 phage infects *E. coli*, it replicates using the host's endogenous enzymes, such as DNA polymerase, ligase, and gyrase, and 11 proteins (pI to pXI) encoded in the M13 genome. There are three stages of RCA (Supplementary Figure S1). In stage 1, pIII on the surface of the M13 phage binds to the F pili of *E. coli* cells. The single-strand phage scaffold DNA (+ strand) enters the cytoplasm and is converted into double-stranded DNA, called the replication form (RF), which consists of (+) and (–) strands DNA. In stage 2, *E. coli* DNA polymerase III binds to the RF DNA, separates the (+) strand from the (–) strand, and synthesizes a new (+) strand DNA using the (–) strand DNA as the template to form the RF DNA. The previously separated (+) strand DNA is also used as a template for DNA polymerase III to form newly synthesized RF DNA (18–21). This newly formed RF DNA interacts with DNA polymerase III to produce RF and (+) DNA. Overall, one RF and (+) DNA are newly produced in each cycle from one RF DNA during stage 2. This stage continues until protein V (pV), a phage protein, accumulates to a threshold concentration (22,25). In stage 3, the RF DNA generated in stage 2 continues to replicate itself and generates one (+) strand DNA. In contrast to stage 2, the separated (+) strand DNA does not participate in DNA synthesis but is exported as phage DNA. At this stage, thousands of pV dimers bind to the (+) strand of DNA to prevent RF formation. These pV–ssDNA complexes also act as an export signal (see Supplementary Figure S1) (26,27). Based on the aforementioned phage replication system, we hypothesized that ssDNA production increases in accordance with the Fibonacci series in stage 2, and an arithmetic increase in stage 3, assuming that DNA replication rate is constant (Supplementary Figure S1). In this context, ssDNA production is dependent on the duration of stage 2, because the rate of Fibonacci increase is greater than that of the arithmetic increase. Herein, we attempted to reduce the pV concentration to induce an extended stage 2 period during the RCA of the M13 phage. Among the various known methods for controlling the expression level of specific proteins, we utilized a 5'-untranslated region (5'-UTR) space sequence modification approach because of the well-recognized role of the spacer region, a 5–6 bp sequence situated between the ribosome binding site (RBS) and start codon of the protein-coding sequence in protein translation (28). Any desired mutations within this region were expected to negatively influence ribosomal binding to the RBS, a process generally understood as a bottleneck in the protein translation process, which should act as an ideal candidate for regulating protein expression (29).

In this study, the RCA replication cycle of the M13 phage was rationally reconfigured to improve M13 phage production. Because of the regulatory role of pV in the RCA replication system, the pV expression level was targeted to rewire RCA regulation. The spacer sequence of pV was mutated to modulate its expression, and the mutant produced approximately 6-fold more phages and ssDNA than did the wild-type strain. The correlation between pV expression levels and phage production was confirmed in two different ways. Therefore, we showed that the reduction of pV expression is a cost-effective method for large-scale production of scaffold DNA, which in turn could potentially reduce the cost

of DNA origami production to approximately €0.22/mg (7000–8600 base-pairing-based structures).

## MATERIALS AND METHODS

### Bacterial strain, plasmids and M13 phage spacer variants

An *E. coli* XL1-blue *recA1 endA1 gyrA96 thi-1 hsdR17 supE44 relA1 lac* [F' *proAB lacIqZΔM15 Tn10* (Tet<sup>r</sup>)] carrying the pZA pLtet::purB vector was used as the host strain. M13mp18 (NEB, Ipswich, MA, USA) was used as the parental phage. All plasmids were cloned using the Gibson assembly kit (NEB). All oligonucleotides were purchased from Bionics (Seoul, Korea) for PCR and sequencing. Q5 polymerase, restriction enzymes, and NEB builder Hifi DNA assembly cloning kits were purchased from NEB.

M13 phage spacer variants were cloned using the Gibson assembly. Two PCR fragments obtained using the appropriate primers (see Supplementary Figure S2) were mixed in appropriate volumes according to the Gibson Assembly<sup>®</sup> Protocol (NEB). PCR products from primers 1-fwd and 1-rev had a library size of 71 variants.

### Bacterial cultivation

Bacterial growth was calculated from the optical density of a 10- or 100-fold diluted suspension at 600 nm, and the optical density was measured using a Du730 UV-vis spectrophotometer (Beckman Coulter, Brea, CA, USA). The following formula was used to calculate bacterial growth:

$$\begin{aligned} 1 \text{ OD} &= 1 \times 10^9 \text{ cells/ml} \\ &= 0.3 \text{ g dry cell weight DCW/l} \end{aligned}$$

The 2XM9 medium (20 g/l glucose, 12 g/l Na<sub>2</sub>HPO<sub>4</sub>, 6 g/l KH<sub>2</sub>PO<sub>4</sub>, 1 g/l NaCl, 2 g/l NH<sub>4</sub>Cl, 1.7 g/l citrate, 2 mM MgSO<sub>4</sub>·7H<sub>2</sub>O, 0.1 mM CaCl<sub>2</sub>, 3.16 mg/l (NH<sub>4</sub>)<sub>6</sub>Mo<sub>7</sub>O<sub>24</sub>·4H<sub>2</sub>O, 24.7 mg/l H<sub>3</sub>BO<sub>3</sub>, 7.13 mg/l CoCl<sub>2</sub>·6H<sub>2</sub>O, 1.59 mg/l CuSO<sub>4</sub> anhydrous, 15.83 mg/l MnCl<sub>2</sub>·4H<sub>2</sub>O, 2.87 mg/l ZnSO<sub>4</sub>·7H<sub>2</sub>O, 1.39 mg/l FeSO<sub>4</sub>·7H<sub>2</sub>O, 0.2 μg/ml doxycycline, and 50 μg/ml chloramphenicol) was used for both bacterial culture and fermentation. The feeding solution added during fermentation contained 500 g/l glucose and 0.2 M MgSO<sub>4</sub>·7H<sub>2</sub>O with 0.2 μg/ml doxycycline and 50 μg/l chloramphenicol.

For culture preparation, the first seed was cultivated in LB (Luria-Bertani broth, BD, Franklin Lakes, NJ, USA) and transferred to a second seed culture in 5 ml of 2XM9. For flask culture, the second seed was scaled up to 25 ml of 2XM9 in 250 ml flasks (initial optical density = 0.125) and incubated at shaking conditions of 250 rpm and 37°C for 24 h.

### Phage and ssDNA separation and quantification

Host *E. coli* cells were centrifuged for 1 h at 7370 rcf and 4°C. The supernatant was taken and incubated for 1 h after adding 0.2 volumes of 30% PEG8000 and 3 M NaCl. After incubation, the mixture was re-centrifuged for 1 h at 7370 rcf and 4°C. The precipitated phage was suspended in 1 ml of TE buffer. Phage quantification was determined from the absorbance at 269 nm and 320 nm, and the absorbance of

the samples was measured using a microplate reader (Synergy H1, BioTek, Winooski, VT).

$$\text{Virions/ml (PFU)} = (A_{269} - A_{230}) \times \frac{6 \times 10^{16}}{\text{number of bases in the phage genome}}$$

The phages were lysed by adding 2 volumes of lysis buffer (1% SDS and 0.2 M NaOH) and incubating the sample in a 70°C water bath for 1 h. After cooling to 25°C, a 1.5 volume of neutralization buffer (3 M sodium acetate) was added and incubated on ice for 1 h, followed by centrifugation for 1 h at 16 000 rcf and 4°C. The supernatant was transferred to a new tube, and two volumes of NT1 binding buffer (Macherey-Nagel, Düren, Germany) were added. The mixture was loaded onto a spin column (Exprep plasmid SV mini, Geneall Biotechnology, Seoul, Korea) and washed with NT3 buffer (Macherey-Nagel). Finally, an appropriate amount of TE buffer (10 mM Tris, 1 mM EDTA) was used to elute the DNA. ssDNA concentration was calculated from the A260 values measured using a nano spectrometer (Nanovue, GE Healthcare, Chicago, IL, USA) according to the following formula:

$$A_{260} \text{ Unit} = 33 \mu\text{l/ml ssDNA}$$

### Quantification of fluorescence protein expression

One milliliter of *E. coli* cell suspension was collected at 6 and 9 h during flask cultivation. After centrifugation, the supernatants were discarded, and the cell pellets were re-suspended in PBS buffer (8 g/l NaCl, 0.2 g/l KCl, 1.44 g/l Na<sub>2</sub>HPO<sub>4</sub>, 0.24 g/l KH<sub>2</sub>PO<sub>4</sub>). The green fluorescence of each cell sample was measured using a plate reader (Synergy H1) at excitation and emission wavelengths of 485 and 528 nm, respectively. The fluorescence of each strain was normalized to its optical cell density (OD600). For the microplate experiment, cells were inoculated and cultured in a plate at 37°C with shaking at 285 rpm until the stationary phase. The cell density and fluorescence were measured every 15 min and normalized.

### Fermentation condition

Fermentation was conducted in a 3 l stirred tank bioreactor (BioCNS, Daejeon, Korea) with a working volume of 1 l. Fermenter seeds were inoculated with an initial OD of 0.125 and cultivated in 2XM9 medium at 800 rpm agitation at 37°C. Fresh air (5 vvm) was supplied at the beginning of fermentation until the early exponential phase and changed to pure O<sub>2</sub> (3 vvm) until the end of the fermentation. Alkaline buffer (50% NH<sub>4</sub>OH) was used to maintain the pH at 6.65–6.75. All chemicals were purchased from Merck (Darmstadt, Germany).

### Folding and analysis of barrel-shaped DNA origami

The staple oligonucleotides for barrel-shaped DNA origami, summarized in Supplementary Figure S4 and Table S2, were purchased from Bioneer (Daejeon, Korea). The M13mp18 scaffold strand (wild-type), used as a control, was purchased from Guild BioSciences (Dublin, OH).

For DNA origami, 10 nM scaffold strands were mixed with a 10-fold excess of staple oligonucleotides in 1× TBE buffer (89 mM Tris, 89 mM boric acid and 2 mM EDTA) with 16 mM MgCl<sub>2</sub>. This mixture was then subjected to a thermal ramp using a Tetrad 2 Peltier thermal cycler (Bio-Rad, Hercules, CA) as follows: 80°C for 15 min followed by a temperature decrease from 60 to 24°C for 36 h.

DNA origami quality was analyzed by electrophoresis on a 1.85% agarose gel containing 0.5× TBE buffer, 16 mM MgCl<sub>2</sub>, and 1× ethidium bromide. Samples (20 μl) were loaded onto the gel after mixing with 5 μl of 5× gel loading buffer. The samples were electrophoresed at 60 V for 1.5 h. The individual bands were visualized with ultraviolet light and imaged using a Gel Doc XR+ gel documentation system (Bio-Rad). To recover the assembled DNA origami for transmission electron microscopy (TEM) imaging, the leading bands were cut out from the gel and extracted using a DNA gel extraction spin column (Bio-Rad).

### Negative-staining TEM analysis

For TEM imaging, 5 μl of each sample was drop-casted onto glow-discharged Formvar-supported carbon TEM grids (Electron Microscopy Sciences, Hatfield, PA, USA). After incubation for 4 min, the solution was drained using filter paper (Whatman, Little Chalfont, United Kingdom). Then, 5 μl of aqueous uranyl formate (Polysciences, Warrington, PA, USA) solution (2% w/v) was added, followed by incubation for 1 min. Finally, the residual uranyl formate solution was removed using filter paper. After thoroughly removing the solution, the samples were imaged using an H-7100 (Hitachi, Tokyo, Japan) operated at 100 kV.

## RESULTS

### Mutation on spacer of pV is effective in scaffold DNA production

As per our hypothesis, we randomly mutated the spacer sequence of the gene encoding pV and attempted to select mutants that enhanced M13 phage production by decreasing pV expression levels. Before mutating the spacer region of the pV-encoding gene, we inserted the kanamycin resistance marker into M13mp18 for the convenience of the following experiment and named the phage M13mp18k-0 (Supplementary Figure S2). We then identified the exact location of the RBS of pV using the UTR designer program (Figure 1A) (29), which indicated that the spacer sequence was TCACA. We attempted to randomize this sequence using a polymerase chain reaction (PCR) and Gibson assembly (see Materials and Methods and Supplementary Figure S2). In total, 71 M13 phage mutation libraries were collected. The number after M13mp18k denotes the sequential number of colonies. The mutated sequences are listed in Supplementary Table S1.

Phage production by the strains containing mutated phage DNA was measured (Supplementary Figure S3) and four mutated phage DNAs (M13mp18k-5, 7, 10, 62) that generated higher levels of phages than M13mp18k-0 were selected. There were no differences in growth rates between wild-type and mutant phages (Figure 1B). Among the four

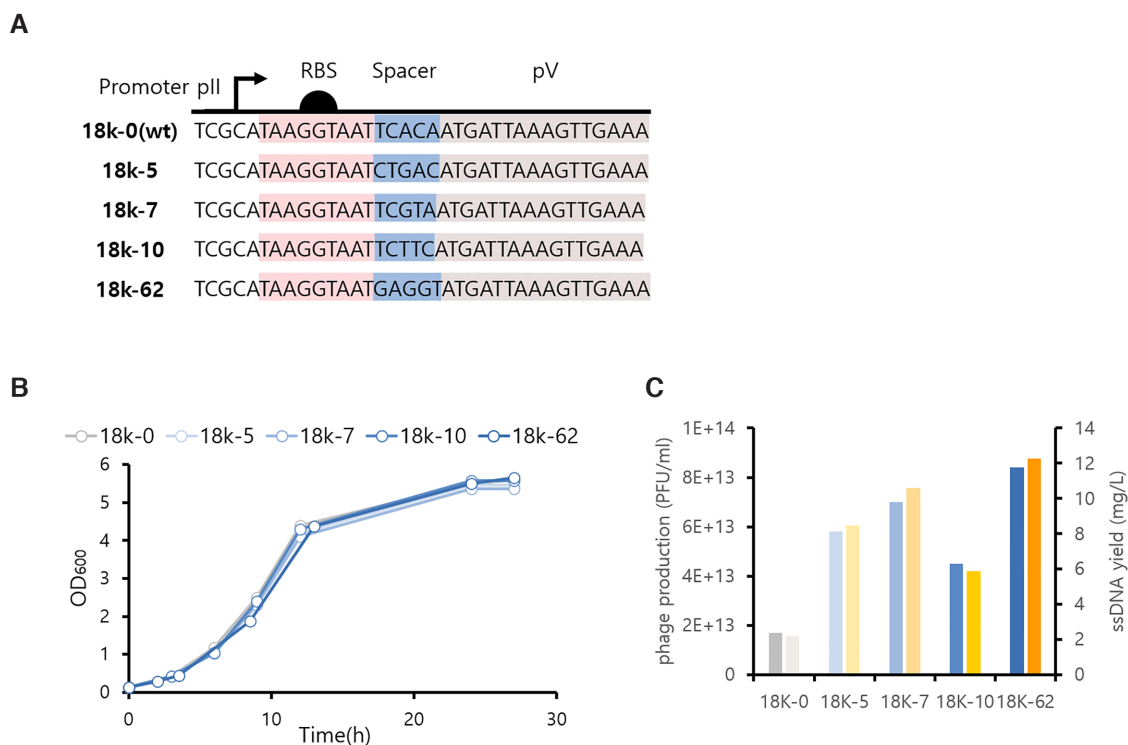


**Figure 1.** Translational repression of phage protein V (pV) enhanced M13 phage and single-strand DNA (ssDNA) production. (A) Sequences of changed scaffold DNA for screened pV variants. (B) Growth curve of every pV mutants. (C) Phage production and ssDNA yield in 250 ml flasks containing 25 ml of 2XM9 media.

mutants, M13mp18k-62, corresponding to the space sequence change from TCACA to GAGGT, showed the most significant increase in phage and ssDNA production (Figure 1C). These results proved that mutations in the pV spacer region are effective in improving phage and ssDNA production by modulating RCA.

#### Variations in a 5 bp spacer sequence of the phage affected pV expression

To investigate the effect of mutated spacers on pV expression levels, reporter vectors were constructed. Each reporter vector contained different spacer sequences between the RBS and the translational initiation site of pV, which was fused to an enhanced green fluorescence protein (EGFP). EGFP is a commonly used reporter protein for observing protein expression levels and was thus used in this study to monitor the pV expression levels associated with mutated spacer sequences. The EGFP-encoding gene was inserted into the C-terminal region of the pV-encoding gene in these vectors (Figure 2A). Assuming that reduced pV expression led to a similar increase in phage production, four M13 phage variants exhibiting enhanced phage production (M13mp18k-5, 7, 10 and 62) and five variants that suppressed phage production (M13mp18k-18, 23, 32, 40 and 59) were selected to construct reporter vectors among the 71 mutants. The spacer sequence of M13mp18k-0 (wild-type) was used as the control, whereas the mutants with diminished phage production, M13mp18k-18, 23, 32, 40 and 59 were used as the comparative group.

Figure 2B and C shows the observed fluorescence levels of each reporter vector normalized to the bacterial cell OD under two different growth conditions. Data in Figure 2B were obtained following cultivation in 250 ml flasks under aerobic conditions at two time points, 6 and 9 h. Data in Figure 2C were continuously measured in a 96-well microplate under semi-anaerobic conditions for 10 h. The normalized fluorescence levels of the reporter vectors of enhanced phage producers (M13mp18k-5, 7, 10, 62) were significantly lower than those of the wild-type, indicating that pV expression levels were significantly reduced in these strains. In particular, M13mp18k-62, the variant exhibiting the highest phage-production ability, showed the lowest fluorescence level in both flask and microplate cultivation. Meanwhile, the fluorescence of the comparative group was higher than that of the control (Figure 2B, C). M13mp18k-23 and 59, which created the smallest amounts of phages during the screening step, showed much higher levels of fluorescence than did 18k-0 (Figure 2B and C). Our data showed that 5 bp spacer sequence variations in the phage affected pV expression, and the expression levels tended to inversely correlate with phage production in *E. coli* infected with the vector.

#### Expression levels of pV were inversely correlated with phage production

The relationship between pV expression levels and phage production was confirmed by additional experiments using an inducible promoter. In this experiment, pV expression was controlled separately from M13 phage production. For this purpose, the pV-encoding gene was deleted from the

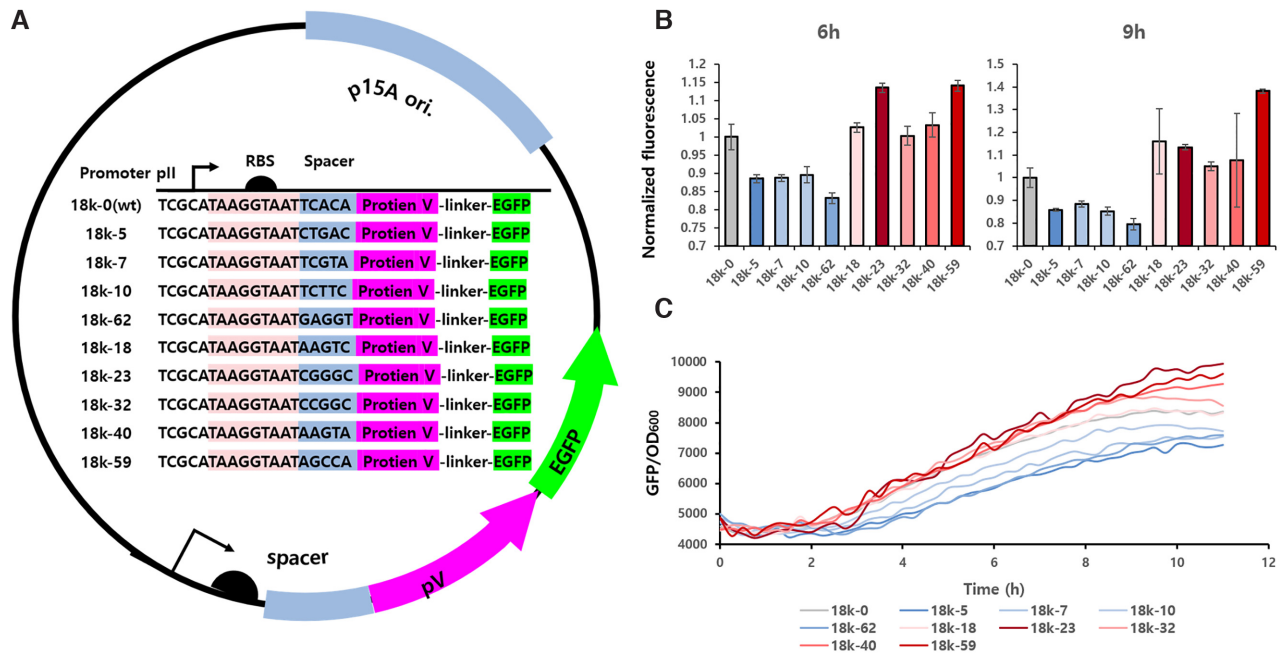


**Figure 2.** Mutation on spacer decreased following gene expression. (A) Vector construct of each mutant. (B) Green fluorescence normalized to cell density during 250 mL flask cultivation for 6 and 9 h, (C) or during cultivation in a 96 well microplate for 10 h.

phage (Figure 3A, M13mp18k  $\Delta$ pV), and it was cloned into an independent plasmid under the pBad promoter (Figure 3A, p15A pBad::pV). The protein expression level under the promoter was controlled by arabinose concentrations in the medium. As previously explained, the pV concentration is a signal for exporting the phage (i.e. Stage 3 of the RCA). Therefore, when *E. coli* was infected with M13mp18k  $\Delta$ pV alone, no phage was detected in the medium, as expected (data not shown). When the inducible pV expression vector, p15A pBad::pV, was introduced into *E. coli* together with M13mp18k  $\Delta$ pV, a phage harboring a single-stranded M13mp18k  $\Delta$ pV was detected in the medium. Because the pBad promoter controls the protein expression level based on the arabinose concentrations, various arabinose concentrations were added to the medium. Increasing the pV expression level via increased arabinose concentrations decreased M13mp18k  $\Delta$ pV production due to an early shift from stage 2 to 3 of the RCA (Figure 3B). These results additionally proved that reduced pV expression improved phage production by controlling the stages of RCA. Additionally, they showed that the pV expression level was the key factor for improving phage production. Therefore, a simple change in the scaffold sequence led to high production of scaffold DNA.

### Large-scale fermentation and folding origami

For large-scale and economic production of the M13 genome as scaffold DNA, *E. coli* fermentation was performed using M13mp18k-0 and M13mp18k-62 phages in a 1 l stirred tank reactor (Supplementary Figure S4). Under glucose fed-batch fermentation, a cell dry weight of 21.6 g/l was obtained after 24 h. When the broth was analyzed, phage concentrations of  $1.27 \times 10^{15}$  PFU/ml for

M13mp18k-0 and  $9.7 \times 10^{15}$  PFU/ml for M13mp18k-62 were obtained, corresponding to 56.14 mg/l (M13mp18k-0) and 268.41 mg/l (M13mp18k-62) ssDNA after downstream processes, respectively. The growth rates of both strains were almost the same, but the glucose consumed by mp18k-62 (91.5 g/l) was much higher than that consumed by mp18k-0 (49.8 g/l). Both strains stopped growing when acetate accumulated to approximately 10 g/l. The phage and ssDNA produced were comparable to those previously reported using high-cell-density cultivation (23), whereas phage and ssDNA titers per cell mass in this study were 2.5 times higher than those previously reported. Finally, we profiled the robustness of the mutated phage DNA (M13mp18k-62) for DNA origami. Using M13mp18k-62 as a scaffold, we folded nanobarrel-shaped DNA structures (Figure 4A) (30) as a representative example of DNA origami (see detailed structural information in Supplementary Figure S5 and Table S2). These nanobarrels were designed to have a diameter and height of 30 nm via coaxial stacking of DNA duplex rings. For a direct comparison, we also folded the same DNA origami with wild-type scaffolds (i.e. M13mp18 from Guild BioSciences). Herein, the collective set of staple strands, used in folding both our mutated scaffolds and commercially available counterparts, was designed to be consistent.

Agarose gel electrophoresis results showed that the DNA nanobarrels folded from the mutated scaffolds formed a distinct band, rather than the diffused leading band (Figure 4B). It turned out that the nanobarrels folded from M13mp18k-62 scaffolds migrated more slowly along the gel line than those from the wild-type scaffolds due to their long single-stranded loop structures. The negative staining-assisted TEM imaging of the solutions, which were selectively abstracted from the corresponding gel band, con-

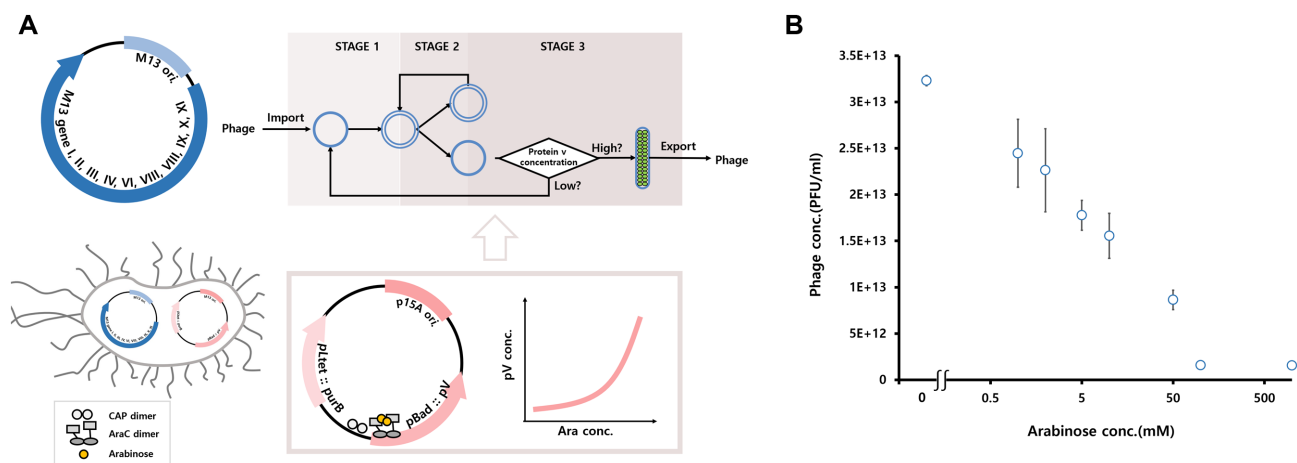


**Figure 3.** Artificial phage protein V (pV) expression change affects phage production. **(A)** Vector construction for separating the expression of pV and the M13 phage genome production (blue, M13mp18ΔpV), enabling the independent expression of pV using the arabinose-induced pBad promoter (pink, p15A pBad::pV). Scheme for the interaction of both vectors. **(B)** Relationship between phage production and arabinose concentration.

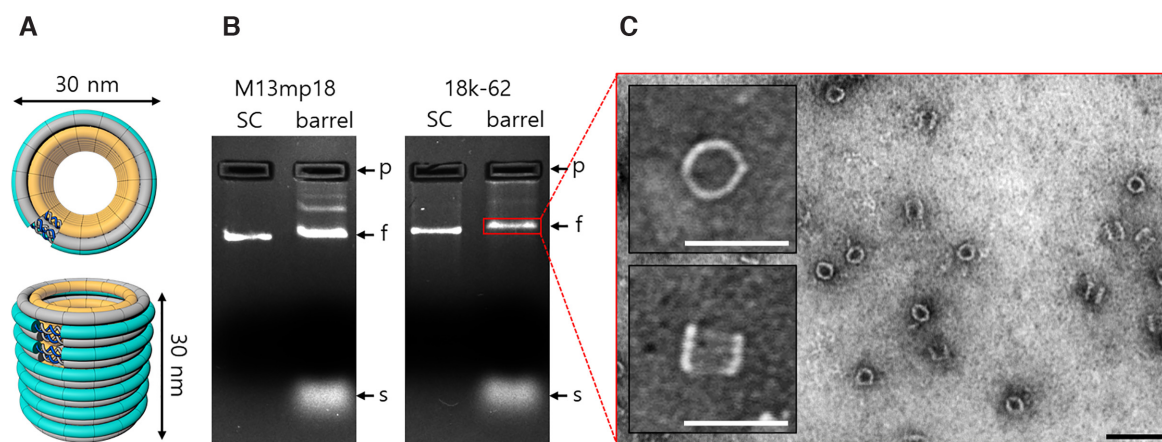


**Figure 4.** Analysis of barrel-shaped DNA origami assembled from mutated phage DNA (M13mp18k-62). **(A)** Schematic illustration of the barrel-shaped DNA origami as a model system. **(B)** Image of agarose gel electrophoresis results for scaffold strands (SC, first lane) and folded barrel (second lane). The fastest migrating band (red box) was extracted and purified for imaging. The 'p,' 'f' and 's' labels indicate the pocket, folded structures, and excess staple strands, respectively. **(C)** Representative transmission electron microscope image of the barrel-shaped DNA origami. White scale bars, 50 nm; black scale bar, 100 nm.

firmly that highly monodisperse DNA nanobarrels matching with the caDNA design were obtained without compromising folding quality (see additional TEM images captured at low magnification; Supplementary Figure S6). Overall, we concluded that mutated phage DNA is comparable to its wild-type counterparts in terms of folding DNA origami structures.

## DISCUSSION

In this study, we described a new means of improving the throughput of scaffold ssDNA production by elongating stage 2 of the M13 replication cycle. By mutating the untranslated region of pV, the expression level of pV was successfully reduced and the resultant ssDNA production was improved. In particular, the expression level of the pV variant was monitored using a fluorescence protein fused to pV, confirming the negative correlation between pV expression and phage production. These observations were fur-

ther verified by regulating pV expression with an inducible promoter, indicating the key role of pV in enhancing the phage production rate. We also attempted to control the expression levels of pII and pX for elongating stage 2. As expected, these experiments also resulted in increased production of ssDNA, but the effects were not as significant as those for the repression of pV (data not shown). In conclusion, the pV-mutated phage showed a different phenotype in *E. coli* by manipulating its regulation system for the stage shift in the replication cycle. Adjusting the replication system of the phage itself, rather than the host system, is assumed to enhance the production of ssDNA. Moreover, it suggests that there are other sequence mutants that may improve phage production. Additionally, enhanced phage and ssDNA production was confirmed using a high-cell-density fermentation method. The ssDNA titer by this fermentation was 2.5-fold higher than that reported in a previous study (17). Finally, we confirmed that the mutated scaffold DNA could be successfully utilized for the folding of

DNA origami structures without compromising structural integrity.

As mentioned in the introduction, the previously reported biotechnological production of DNA origami opened the way for an affordable production cost for relatively small DNA origami (i.e., €0.18/mg for structures with <3200 bp) (17). However, this biotechnological approach has not yet been validated for conventional M13-based ssDNA with 7000–8600 bases, which have been used as a commodity scaffold. Thus, our strategy could be adopted as a good complement for cost-effective production of scaffold DNA. Indeed, we can estimate that the production cost of the DNA origami folded with 7000–8600 base scaffolds could be decreased to approximately €0.22/mg when our method is applied in a pilot-scale stirred tank bioreactor with similar manufacturing capability and environment as in previously reported cost estimations for small DNA origami (17), along with biotechnological production of staple ssDNA.

Furthermore, it is important to note that staple strands have become commercially affordable, because the costs of chemically synthesized oligonucleotides have decreased over the past few years. For example, 10–50 base-long oligonucleotides with custom sequences can be chemically synthesized and purchased at €4.9/mg (from list price at Bioneer). Assuming that 50% of DNA origami is made up of staple strands, and molar excess (2.5:1) of staple strands over scaffold strands is used, the estimated price of chemically synthesized staple strands for 1 mg DNA origami is €6.1, which is far less than the previously reported estimation (i.e., €96.5/mg) (17). Considering such improvements, developing a new route for the efficient production of scaffold DNA can have special significance for the economical production of DNA origami. Indeed, combined with chemically synthesized oligonucleotides, our efficient scaffold strand production method could reduce the production cost of DNA origami to €15/mg even at liter-scale ssDNA production, which is already competitive with biotechnological production of smaller DNA origami (€23/mg at liter-scale production). Taken together, rewiring the RCA regulation of M13 phage replication can be an efficient way to enhance the throughput of scaffold DNA production, facilitating the use of DNA origami as a go-to-tool. These experimental results are expected to offer economic benefits in the field of DNA origami.

## SUPPLEMENTARY DATA

[Supplementary Data](#) are available at NAR Online.

## FUNDING

This research was supported by Future Materials Discovery Program through the National Research Foundation of Korea (NRF) funded by Ministry of Science and ICT (NRF-2017M3D1A1039421 and NRF-2017M3D1A1039423). Funding for open access charge: Future Materials Discovery Program through the National Research Foundation of Korea (NRF) funded by Ministry of Science and ICT (NRF-2017M3D1A1039421 and NRF-2017M3D1A1039423).

*Conflict of interest statement.* None declared.

## REFERENCES

- Rothemund, P.W.K. (2006) Folding DNA to create nanoscale shapes and patterns. *Nature*, **440**, 297–302.
- Douglas, S.M., Marblestone, A.H., Teerapittayanon, S., Vazquez, A., Church, G.M. and Shih, W.M. (2009) Rapid prototyping of 3D DNA-origami shapes with caDNAno. *Nucleic Acids Res.*, **37**, 5001–5006.
- Dietz, H., Douglas, S.M. and Shih, W.M. (2009) Folding DNA into twisted and curved nanoscale shapes. *Science*, **325**, 725–730.
- Han, D.R., Pal, S., Nangreave, J., Deng, Z.T., Liu, Y. and Yan, H. (2011) DNA origami with complex curvatures in three-dimensional space. *Science*, **332**, 342–346.
- Benson, E., Mohammed, A., Gardell, J., Masich, S., Czeizler, E., Orponen, P. and Hogberg, B. (2015) DNA rendering of polyhedral meshes at the nanoscale. *Nature*, **523**, 441–444.
- Wagenbauer, K.F., Sigl, C. and Dietz, H. (2017) Gigadalton-scale shape-programmable DNA assemblies. *Nature*, **552**, 78–83.
- Hong, F., Zhang, F., Liu, Y. and Yan, H. (2017) DNA Origami: scaffolds for creating higher order structures. *Chem. Rev.*, **117**, 12584–12640.
- Douglas, S.M., Bachelet, I. and Church, G.M. (2012) A logic-gated nanorobot for targeted transport of molecular payloads. *Science*, **335**, 831–834.
- Gerling, T., Wagenbauer, K.F., Neuner, A.M. and Dietz, H. (2015) Dynamic DNA devices and assemblies formed by shape-complementary, non-base pairing 3D components. *Science*, **347**, 1446–1452.
- Kopperger, E., List, J., Madhira, S., Rothfischer, F., Lamb, D.C. and Simmel, F.C. (2018) A self-assembled nanoscale robotic arm controlled by electric fields. *Science*, **359**, 296–300.
- Jiang, Q., Song, C., Nangreave, J., Liu, X.W., Lin, L., Qiu, D.L., Wang, Z.G., Zou, G.Z., Liang, X.J., Yan, H. *et al.* (2012) DNA Origami as a carrier for circumvention of drug resistance. *J. Am. Chem. Soc.*, **134**, 13396–13403.
- Perrault, S.D. and Shih, W.M. (2014) Virus-inspired membrane encapsulation of DNA nanostructures to achieve in vivo stability. *ACS Nano*, **8**, 5132–5140.
- Li, S.P., Jiang, Q., Liu, S.L., Zhang, Y.L., Tian, Y.H., Song, C., Wang, J., Zou, Y.G., Anderson, G.J., Han, J.Y. *et al.* (2018) A DNA nanorobot functions as a cancer therapeutic in response to a molecular trigger in vivo. *Nat. Biotechnol.*, **36**, 258–264.
- Kuzyk, A., Schreiber, R., Zhang, H., Govorov, A.O., Liedl, T. and Liu, N. (2014) Reconfigurable 3D plasmonic metamolecules. *Nat. Mater.*, **13**, 862–866.
- Lee, J., Huh, J.H., Kim, K. and Lee, S. (2018) DNA Origami-guided assembly of the roundest 60–100 nm gold nanospheres into plasmonic metamolecules. *Adv. Funct. Mater.*, **28**, 1707309.
- Fang, W.N., Jia, S.S., Chao, J., Wang, L.Q., Duan, X.Y., Liu, H.J., Li, Q., Zuo, X.L., Wang, L.H., Wang, L.H. *et al.* (2019) Quantizing single-molecule surface-enhanced Raman scattering with DNA origami metamolecules. *Sci. Adv.*, **5**, eaau4506.
- Praetorius, F., Kick, B., Behler, K.L., Honemann, M.N., Weuster-Botz, D. and Dietz, H. (2017) Biotechnological mass production of DNA origami. *Nature*, **552**, 84–87.
- Rakonjac, J., Bennett, N.J., Spagnuolo, J., Gagic, D. and Russel, M. (2011) Filamentous bacteriophage: biology, phage display and nanotechnology applications. *Curr. Issues Mol. Biol.*, **13**, 51–75.
- Horiuchi, K. (1997) Initiation mechanisms in replication of filamentous phage DNA. *Genes Cells*, **2**, 425–432.
- Meyer, T.F. and Geider, K. (1982) Enzymatic-synthesis of bacteriophage-Fd viral-DNA. *Nature*, **296**, 828–832.
- Asano, S., Higashitani, A. and Horiuchi, K. (1999) Filamentous phage replication initiator protein gpII forms a covalent complex with the 5' end of the nick it introduced. *Nucleic Acids Res.*, **27**, 1882–1889.
- Lin, N.S.C. and Pratt, D. (1972) Role of bacteriophage-M13 gene 2 in viral DNA-replication. *J. Mol. Biol.*, **72**, 37–49.
- Kick, B., Praetorius, F., Dietz, H. and Weuster-Botz, D. (2015) Efficient production of single-stranded phage DNA as scaffolds for DNA Origami. *Nano Lett.*, **15**, 4672–4676.
- Kick, B., Hensler, S., Praetorius, F., Dietz, H. and Weuster-Botz, D. (2017) Specific growth rate and multiplicity of infection affect

- high-cell-density fermentation with bacteriophage M13 for ssDNA production. *Biotechnol. Bioeng.*, **114**, 777–784.
25. Guan, Y., Zhang, H. and Wang, A.H.J. (1995) Electrostatic potential distribution of the gene-V protein from Ff-Phage facilitates cooperative DNA-binding - a model of the Gvp-Ssdna complex. *Protein Sci.*, **4**, 187–197.
26. Fulford, W. and Model, P. (1988) Bacteriophage-F1 DNA-eplication genes .2. The roles of gene-V protein and gene-II protein in complementary strand synthesis. *J. Mol. Biol.*, **203**, 39–48.
27. Michel, B. and Zinder, N.D. (1989) Translational repression in bacteriophage-F1 - characterization of the gene-V protein target on the gene-II messenger-RNA. *P Natl Acad Sci USA*, **86**, 4002–4006.
28. Lu, P., Vogel, C., Wang, R., Yao, X. and Marcotte, E.M. (2007) Absolute protein expression profiling estimates the relative contributions of transcriptional and translational regulation. *Nat. Biotechnol.*, **25**, 117–124.
29. Seo, S.W., Yang, J.S., Kim, I., Yang, J., Min, B.E., Kim, S. and Jung, G.Y. (2013) Predictive design of mRNA translation initiation region to control prokaryotic translation efficiency. *Metab. Eng.*, **15**, 67–74.
30. Wickham, S.F.J., Auer, A., Min, J.H., Ponnuswamy, N., Wehrstein, J.B., Schueder, F., Strauss, M.T., Schnitzbauer, J., Nathwani, B., Zhao, Z. *et al.* (2020) Complex multicomponent patterns rendered on a 3D DNA-barrel pegboard. *Nat. Commun.*, **11**, 5768.